Research in Astronomy and Astrophysics, 25:035021 (7pp), 2025 March

https://doi.org/10.1088/1674-4527/adbc7c
CSTR: 32081.14.RAA.adbc7c

Frequency of Occurrence of Solar Plasma Disturbances in Interplanetary Space

Munendra Singh[1] and Y. P. Singh[2]
[1] Department of Physics, SSBSR, Sharda University, Greater Noida, Uttar Predesh, 201310, India; munendra.singh@sharda.ac.in
[2] Institute of Applied Sciences, Mangalayatan University, Aligarh, 202145, India; yatendrapalsingh@gmail.com
Received 2024 October 26; revised 2025 January 30; accepted 2025 February 26; published 2025 March 24

Abstract

Major solar plasma disturbances are subjected to Lomb–Scargle periodogram and wavelet analysis to determine the occurrence frequency. These disruptions include interplanetary coronal mass ejection, sudden storm commencement, high-speed streams, corotating interaction regions, interplanetary shocks and Forbush decreases. We included information on all of the aforementioned solar disturbances for the last six solar cycles, from 1965 to 2023, for this study. Our findings reveal some intriguing and noteworthy results that clearly distinguish between even and odd-numbered solar cycles. The study suggests that the Sun behaves differently in odd and even-numbered solar cycles as it comes from the massive solar eruptions. During even-numbered solar cycles, variations with a period of ∼44 days are prominently observed in addition to solar rotation (∼27 days) and extended solar (∼36 days) rotation. However, in addition to solar rotation, prolonged solar rotation, and periods of around 44 days, we also detect a number of intermittent changes with nearly comparable amplitude during the odd-numbered solar cycles. The findings also demonstrate that, in contrast to odd-numbered solar cycles, the emissions rate of these disruptions is more distinct and predictable during even-numbered solar cycles.

Key words: Sun: activity – Sun: coronal mass ejections (CMEs) – Sun: magnetic fields – Sun: rotation – (Sun:) solar wind

1. Introduction

Coronal mass ejections (CMEs) are the most geoeffective disturbances (Zhang et al. 2007; Shen et al. 2017) of solar eruption in terms of their impact on Earth and it's atmosphere. When a CME encounters the Earth's magnetosphere, a rapid storm begins, resulting in an immediate increase in the strength of the magnetic field near the Earth's surface. A CME triggers interplanetary shocks (IP shocks) as suggested by Oliveira & Raeder (2015). Interplanetary space signatures of CMEs are known as interplanetary coronal mass ejections (ICMEs). An abrupt change in the solar wind's plasma dynamic pressure and surface geomagnetic field's northward indicates the sudden storm commencements (SSCs). These disturbances affect satellites and communication systems and disturb planets' magnetic fields. Solar coronal holes are the usual source of high-speed streams (HSSs), which are significant emissions from the Sun. Coronal holes are regions in the Sun's high latitudes where rapid solar wind can escape. Plasma velocity, density, and temperature of these streams can differ and have a significant impact on the environment surrounding Earth and other planets. Axford & Reid (1963) postulated the genesis and source of high-speed solar wind streams. When high-speed solar wind streams meet sluggish solar wind streams in interplanetary space, they form corotating interaction regions (CIRs), creating an interaction area. The solar wind's dynamic interaction as it rotates with respect to the Sun leads to the initiation of geomagnetic storms. Forbush (1937) first analyzed data collected from ion chambers positioned at various locations on the Earth. He determined that the variation in intensity was caused by the geomagnetic disruptions, termed as Forbush decrease (Fd). In subsequent research, Simpson et al. (1953) documented the same fluctuations in a neutron monitor and Meyer & Simpson (1955) observed oscillations at different altitudes using both a balloon and an airplane.

At the ground level, geomagnetically induced currents (GICs) are the most hazardous disruptions that arise during a geomagnetic storm. They result directly from the extreme temporal fluctuations of the magnetosphere and ionosphere currents, which induce an electric field on the surface of the Earth. Solar plasma disturbances can trigger geomagnetic activities like auroras, disrupt power grids, satellite operations, communication/navigation systems and other climate and atmospheric effects (Pirjola 1982; Tsurutani & Hajra 2021 and references therein). Thus, by comprehending the variations in the abrupt initiation of solar disturbances, we can enhance our ability to predict and alleviate the consequences caused by these disturbances. Furthermore, understanding the variety of storm commencements could be advantageous in taking proactive measures to resolve these disturbances. As a result, such investigation has emerged as a focused and extensive field

of study. Scientists are conducting thorough investigations to identify periodic patterns in these disturbances, aiming to gather information proactively. These studies are important in the fields of solar physics, solar-terrestrial physics, heliospheric physics, and the relationship between the Sun and climate. Because of this, it is essential to use better and more accurate methods to find the possible periodicities of interplanetary disturbances. This could help us learn more about the solar dynamo oscillations. Thus, the study of variation in such disturbances helps us to understand the Sun and its intricate behavior.

The variations in continuous data of solar-wind plasma and field parameters, geomagnetic indices and the cosmic ray intensity indicator are well reported (Axford & Reid 1963; Rieger et al. 1984; Gonzalez & Gonzalez 1987; Mursula & Zieger 2000, Mursula et al. 2003; Nayar et al. 2001, Nayar et al. 2002; Singh et al. 2012; Modzelewska & Alania 2013; Chowdhury et al. 2015; Kudela & Sabbah 2016; Singh 2020 and reference therein). However, variations in discontinuous data from HSSs, coronal mass ejections, Fds and SSCs were reported by Verma & Joshi (1994), Lara et al. (2008), Singh & Badruddin (2024), Singh et al. (2024).

2. Data and Analysis Technique

The data on SSC are freely available at https://isgi.unistra.fr/events_sc.php. We utilize the catalog of Fds and interplanetary disturbances (http://spaceweather.izmiran.ru/eng/dbs.html). We did not consider the Fd events with magnitude $<1.5\%$ in order to avoid any possible interference due to the presence of diurnal variation whose amplitude is usually $<1.5\%$ (Venkatesan & Badruddin 1990; Singh & Badruddin 2006). The catalog of ICMEs from 1996 to 2023 is freely available at https://izw1.caltech.edu/ACE/ASC/DATA/level3/icmetable2.htm. HSS/CIR catalog (1995–2009) is taken from Jian et al. (2011) and that from 2009 to 2019 is available at http://www.geodin.ro/varsiti/. Data on IP shocks from 1995 to 2023 are available at https://zenodo.org/record/7991430. For this study, we selected a total of 5351 events during the examined period. These data include 1387 SSC events from 1965 to 2023; 1818 Fds from 1965 to 2019; 562 ICMEs events from 1996 to 2023; 603 IP shocks from 1995 to 2023; 576 HSS events from 1995 to 2019 and 405 CIRs from 1995 to 2019. Duplicity of events in a day has been removed before proceeding to analysis.

To find the occurrence rate of interplanetary disturbances, we applied a Lomb–Scargle (L-S) periodogram and wavelet analysis procedure during: (a) all even and odd-numbered solar cycles and (b) individual even and odd-numbered solar cycles of the discontinuous data. We used the Morlet wavelet method to study the occurrence rate of plasma disturbances. We obtain results using a single selected maternal function and scaling parameters. Wavelet analysis studies actual time series that are non-stationary in nature because they hide extreme variations, and these fluctuations occur with high frequency. This method is most suitable for handling non-stationary time series and has advantages over traditional Fourier methods, when the signal contains discontinuities. The wavelet power spectrum (WPS) and the global wavelet spectrum (GWS) show exactly how the non-recurrent and recurrent signals of the time series change over time and space in this method. A time series is expanded in terms of time-localized wavelets, and its two-dimensional representation (Torrence & Compo 1998; Morlet et al. 1982) is

$$f(t, t', n) = \exp(2\pi \mathrm{int}) \exp\left\{-n^2 \frac{(t - t')^2}{2}\right\}, \quad (1)$$

where n is the frequency and t' is the delay time.

The time-averaged wavelet spectrum over all the local wavelet spectra (i.e., the GWS) is given by

$$W^2(x) = \frac{1}{N} \sum_{n=0}^{N-1} |W(x)|^2,$$

where $W_n(x)$ is the wavelet power and N is the number of local wavelet spectra.

In the WPS, the colors and contours provide information about the levels of spectral power corresponding to each variation at different time periods. In the wavelet plots, the yellow and green colored areas correspond to lower power regions and dark yellow-colored areas correspond to the regions of greater power, however, blue-colored areas correspond to very low power regions. The colored regions, however, in all the wavelet figures indicate the region of the spectrum below the 95% confidence level while the thick (black line) contours are the regions of the spectrum at the 95% confidence level. In the global power spectrum (right panel) of each wavelet figure (Figures 8 and 9), the variation of power is shown with period and the thick dashed line (yellowish color) in the panel represents the threshold line at the 95% confidence level. A peak in the GWS is considered significant if it touches or is above the dashed line.

3. Results and Discussion

Sudden impulses are induced by tangential discontinuities, while hydromagnetic shocks are the main cause of SSC as reported in Burlaga & Ogilvie (1969). Earlier, Wilson & Sugiura (1961) reported on the hydromagnetic interpretation of these SSCs, while Gerand (1959) examined propagation of SSCs. Using Fourier power spectrum analysis, Lara and his coauthors observed substantial CME periods at 196, 272, and 358 days (Lara et al. 2008). Choudhary and his coauthors in 2014 report several periodicities in the time series of magnetic-flux emergence, solar flares, and CMEs during cycle 23–24 (Choudhary et al. 2014). Just prior to the abrupt onset of geomagnetic storms, there is an increase in the intensity of solar

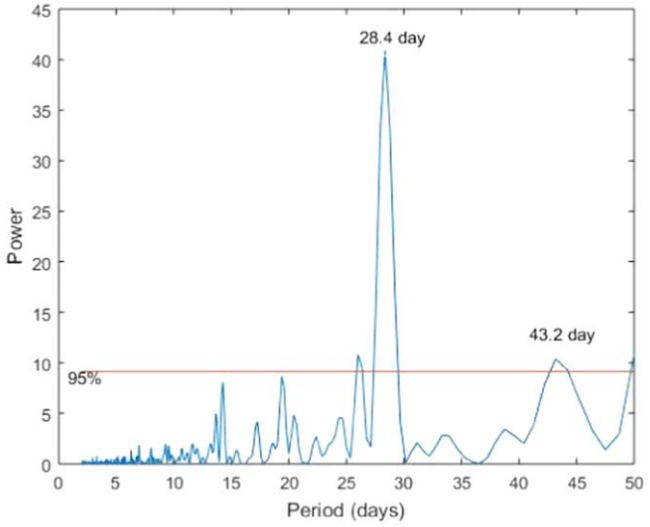

Figure 1. Short-term fluctuations of solar plasma disturbances during cycle 24. The horizontal red line represents a 95% significance level.

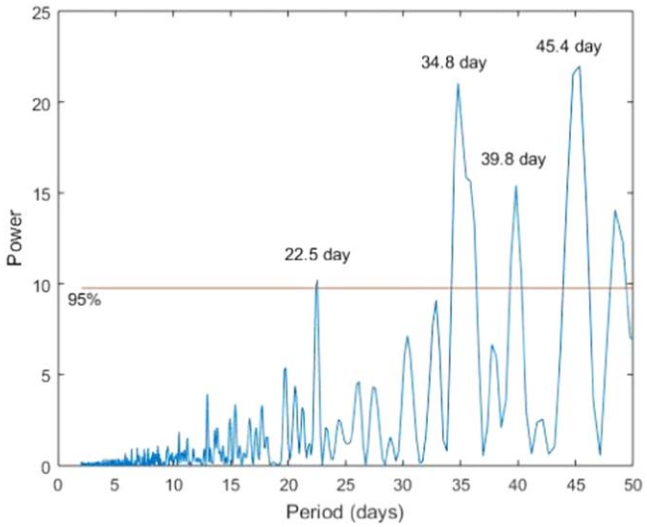

Figure 2. Short-term fluctuations of solar plasma disturbances during cycle 23. The horizontal red line represents a 95% significance level.

cosmic radiation as observed by Axford & Reid (1963). Several other researchers addressed the direction, impact, and spread of IP shock disturbances (Wu & Lepping 2008; Takeuchi et al. 2002; Wilken et al. 1982).

Figure 1 displays the L-S periodogram of solar and interplanetary disturbances during solar cycle 24. A sharp and intense peak around 28.4 days in the periodogram suggest that solar rotation period is very dominating period of solar disturbances during the solar cycle 24. One more variation of 43.2 days significantly appears in the periodogram. The L-S periodogram of interplanetary disturbances during solar cycle 23 is depicted in Figure 2. Five significant variations (22.5, 34.8, 39.8, 45.4 and 49.2 days) are observed in the periodogram. The 22.5 day variation is just significant at the 95% level and appears as minimum power values, however, periods of 34.8, 39.8, 45.4 and 49.2 days appears as significant amplitudes. This indicates that the frequency of occurrence of higher periods of disturbances is more probable. Three significant periods (16.3, 22.9 and 44.8 days) are observed in the periodogram of discontinuous time series of interplanetary disturbances during solar cycle 22 as shown in Figure 3. The 44.8 day period is very intense and has about 2.5 times more peak amplitude than either of the former periods. Figure 4 shows the periodogram of random disturbances that occurred during solar cycle 21. Three short term variations (17.4, 22.7, and 25.8 days) are lower than the solar rotation period (28.6 days). The 43.6 day period is the other significant variation of the time series. The solar rotation period appears with higher amplitude, while a 43.6 day period appears with intermediate power. The remaining three variations appear to have the same amplitude. The L-S periodogram of discontinuous data of disturbances during solar cycle 20 is shown in

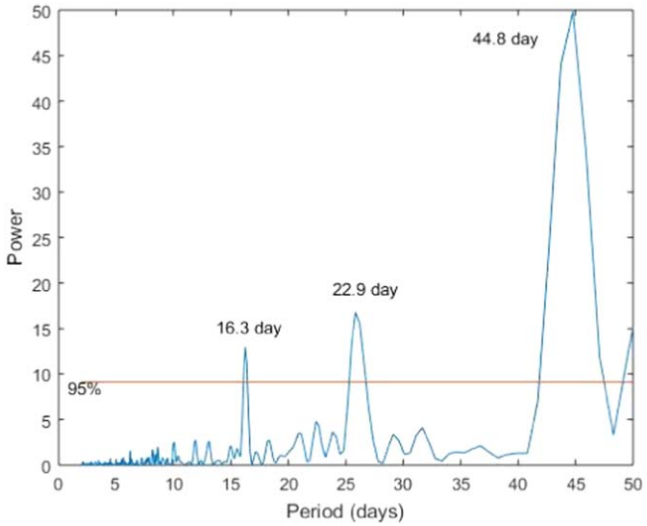

Figure 3. Short-term fluctuations of solar plasma disturbances during cycle 22. The horizontal red line represents a 95% significance level.

Figure 5. The 20 day, 23.7 day, and solar rotation periods appear significantly with almost the same power, while an extended solar rotation period (36.8 days) appears with intermediate peak amplitude. The 43.6 day period is very dominant, which has the maximum peak power value of solar cycle 20. All the observed periods are tabulated in Table 1.

All even and odd cycle wise analyses of the interplanetary disturbances are shown in Figures 6 and 7. Figure 6 is the periodogram of all the selected disturbances observed during both the even-numbered solar cycles (cycle 22 and cycle 24). Short term fluctuations with a 20 day period, near solar rotation

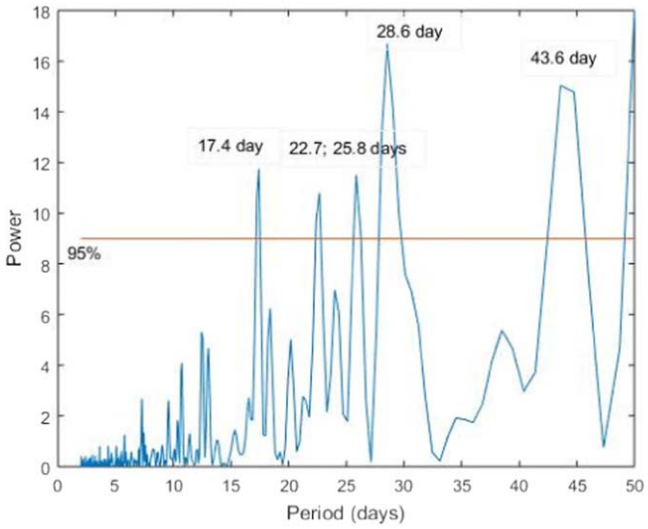

Figure 4. Short-term fluctuations of solar plasma disturbances during cycle 21. The horizontal red line represents a 95% significance level.

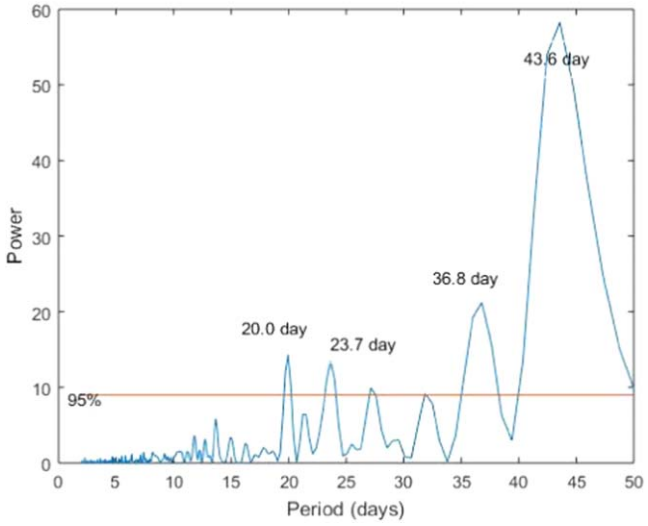

Figure 5. Short-term fluctuations of solar plasma disturbances during cycle 20. The horizontal red line represents a 95% significance level.

periods 24.2, 26.4 and 27.9 days, are appearing in the periodogram with low amplitudes. The 43.2 and 45.7 day periods appeared prominently, while the case with 45.7 days has the highest amplitude among other variations. Large numbers of low amplitude fluctuations are appearing in the discontinuous data of interplanetary disturbances during the odd-numbered solar cycles (cycle 21, cycle 23 and partially cycle 25) as shown in Figure 7. The variations of periods of 22.4 days, extended solar rotation period (35.6 days), 39.8 days, 43.5 days, 45.5 days, and 49.2 days appear with lower amplitudes. However, periods of 51.7, 59.3, 63.2, 72.0

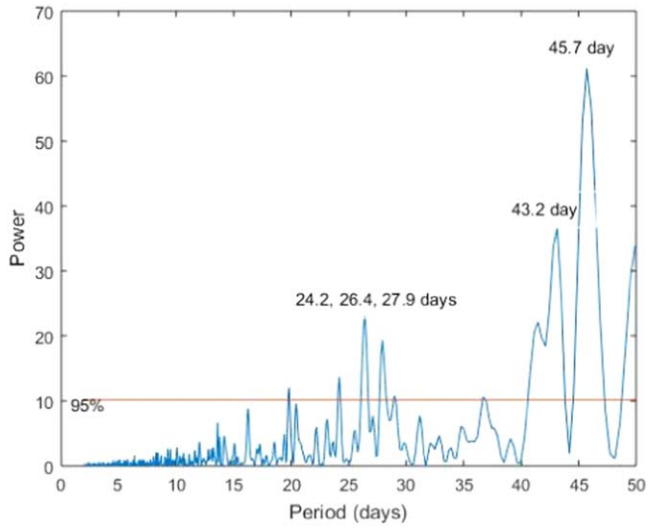

Figure 6. Short-term fluctuations of solar plasma disturbances during even-numbered solar cycles (cycles 20, 22 and 24). The horizontal red line represents a 95% significance level.

Table 1
L-S periodogram Results for Observed Periods (in Days) During Solar Cycles

Cycle 20 Period	Cycle 21 Period	Cycle 22 Period	Cycle 23 Period	Cycle 24 Period
	17.4	16.3		
20.0				
23.7	22.7			
	25.8	25.9		26.3
	28.6			28.4
36.4			34.8	
			39.8	
43.6	43.6	44.8	45.4	43.2
			48.4	

and 82.4 days are the other variations which appear in the periodogram.

We performed wavelet analysis on the solar disturbance time series to support and justify results obtained by using the L-S periodogram technique. Figure 8 is the WPS and GWS of all the selected interplanetary disturbances that occurred during both the even-numbered solar cycles. The GWS of the figure shows three significant variations (27.8, 46.7 and 61.7 days) are observed in the time series. The solar rotation period is just significant, while 46.7 day variation has maximum peak power value. The black contours of this variation and 61.7 days appear throughout the WPS. The WPS and GWS of disturbances selected during the odd-numbered solar cycles are depicted in Figure 9. From the figure it is clear that contours during the odd-numbered solar cycles have larger area compared to the even-numbered solar cycles, hence a

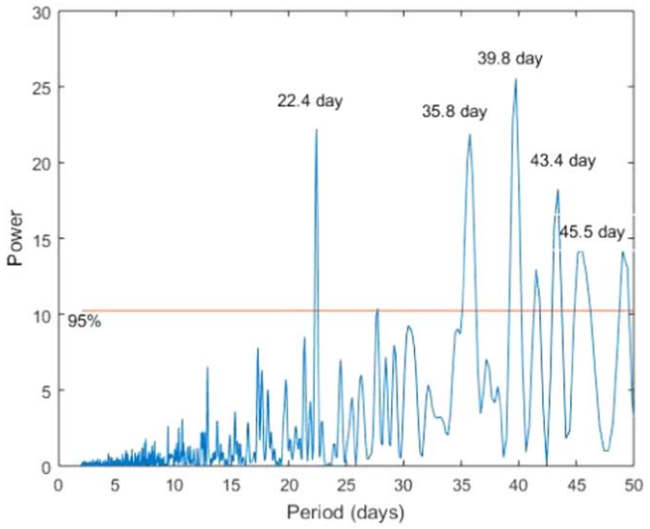

Figure 7. Short-term fluctuations of solar plasma disturbances during odd-numbered solar cycles (cycles 21, 23 and partially 25). The horizontal red line represents a 95% significance level.

significant broad peak (spread from solar rotation period to 90 days) appears in the GWS. These results agree with the results obtained through the L-S periodogram technique.

4. Conclusions

Based on the results obtained from the L-S periodogram and wavelet analysis, we conclude that a period of 44 days is prominently reported in the plasma data. This variation significantly appears in the periodogram as well as in the wavelet power and global power spectra. The L-S periodogram results are well supported by the results obtained using the wavelet technique. Our findings reveal that:

1. A significant and prominent ∼44.0 day period is constantly observed in the time series during both even and odd-numbered solar cycles.
2. During the even-numbered solar cycles, solar rotation, extended solar rotation period and ∼44.0 day periods are prominent. However, during the odd-numbered solar cycles, other than these periods, intermittent periods equally appeared.
3. Only well-known fluctuations are observed in the time series during the even-numbered solar cycles, however, a significant number of intermittent periods other than well-known periods are observed during the odd-numbered solar cycles.
4. Our results show, in contrast to odd-numbered solar cycles, the emission rates of considered plasma disturbances are smoother and more predictable during even-numbered solar cycles.
5. The period of ∼22.0 days is significantly observed during solar cycles 20, 21 and 23. This variation could be the first sub-harmonic of the ∼44.0 day variation.

As per the literature survey, the ∼45 day period was first reported by Madden & Julian (1971). Authors examined daily rawinsonde data for Canton Island using spectrum and cross-spectrum analysis and reported a very pronounced maximum in the co-spectrum of the 850 and 150 mb zonal wind components in the frequency range $0.0245\,\mathrm{day}^{-1}$ to $0.0190\,\mathrm{day}^{-1}$ (41–53 day period). Kaynano & Kousky (2002) used extended empirical orthogonal function analyses and reported the evolution of the 30–60 day intraseasonal including Madden-Julian oscillation (MJO), during boreal winter and summer. Authors also observed patterns that describe an eastward traveling large−scale oscillatory regime with a period of ∼45 days.

Singh et al. (2024) reported a significant 44.2 day period in addition to an extended solar rotation period in SSC time series from 1869 to 2023. Authors found 31.3 and 48.7 day periods and 22.4 and 43.6 day periods of SSC during even− and odd −numbered solar cycles. During the negative polarity state of the heliosphere, solar rotation period (31.3 days) and a period of 44.2 days was observed in SSC. Singh & Badruddin (2024) found 41.8 day and 62.5 day periods in the Fds during even-numbered solar cycles and 30.0 day and 46.7 day periods during selected odd-numbered solar cycles. Significant 42.2 day and 43.0 day periods are reported in Fds during positive and negative polarity states of the heliosphere respectively. However, these fluctuations, which are regular (systematic) or irregular (random), were not reported in the previous studies.

Kilcik et al. (2024) reported 44–45 day periodicity within the multi-taper method spectrum of CI, Dst, CRI, and CME number data sets, and it is verified by the wavelet scalograms of the FI, CI, Ap, Dst, and CRI data sets during the maximum phase of the solar cycle. Consequently, we may assert that the primary origin of this periodicity is the eruptive solar phenomena, including coronal mass ejections and solar flares visible on the Sun. The ∼43, ∼45 and ∼47 day periods are well reported in sunspot numbers and sunspot areas, ∼45 day period in 10.7 cm solar radio flux, ∼44 day period in the B_z component of the interplanetary magnetic field along with ∼45 day period in geomagnetic index Ap as reported by Chowdhury et al. (2015). Authors also reported a significant ∼40 day period in the sunspot area and sunspot numbers from the end of 2011 to the onset of 2013 and early 2011 to around the end of 2013 respectively. Earlier, significant peaks at ∼41 days were detected in flare and sunspot area data during solar cycle 22 as reported by Bai (1992), Chowdhury et al. (2014). Lou et al. (2003) reported a ∼43 day period in the flare data during the ascending phase of cycle 23. As many authors have significantly observed this period in many solar wind

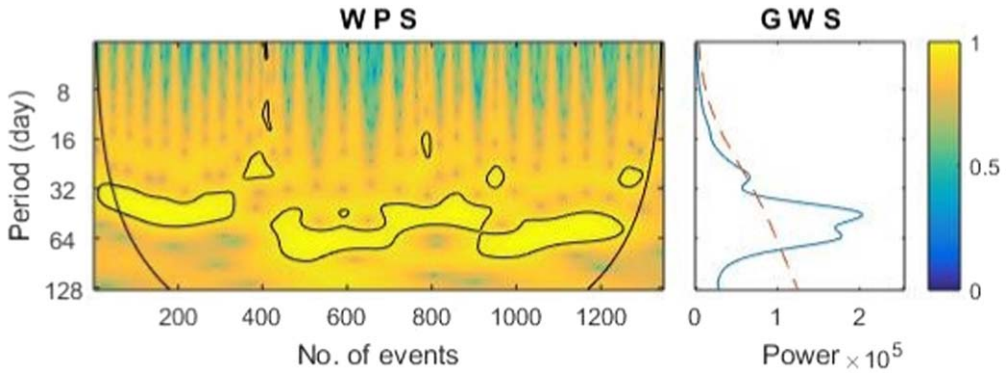

Figure 8. WPSs and GWSs of solar plasma disturbances across all even-numbered solar cycles. The wavelet spectra are color-coded: the dark-yellow regions correspond to maximum power, and a black contour shows the cone of influence of the spectra. The normalized GWSs are shown on the right of each panel. In this case the dashed line represents confidence levels above 95%. Density of power is also shown in the column-color-bar.

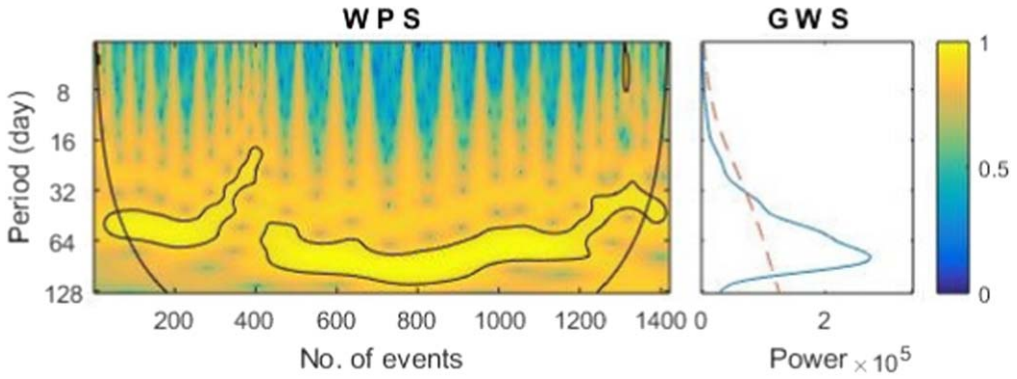

Figure 9. WPSs and GWSs of solar plasma disturbances across all odd cycles. The wavelet spectra are color-coded: the dark-yellow regions correspond to maximum power, and black contour shows the cone of influence of the spectra. The normalized GWSs are shown on the right of each panel. In this case the dashed line represents confidence levels above 95%. Density of power is also shown in the column-color-bar.

plasma parameters like solar flares index, CMEs, sunspot numbers, sunspot areas, time series of Fd, SSC, cosmic ray intensity, and geomagnetic activity index. This periodicity could stem from a solar phenomenon because it interferes with the propagation of cosmic rays in the heliosphere and disturbs geomagnetic activity. Hence, this period appears to require attention in space weather applications.

Acknowledgments

We gratefully acknowledge the use of the catalog of sudden storm commencement events from https://isgi.unistra.fr/events_sc.php, Fds and interplanetary disturbances from http://spaceweather.izmiran.ru/eng/dbs.html, ICMEs from https://izw1.caltech.edu/ACE/ASC/DATA/level3/icmetable2.htm, high speed solar wind plasma streams and corotating interaction regions from http://www.geodin.ro/varsiti/ and interplanetary shocks from https://zenodo.org/record/7991430. Wavelet software provided by C.T. and G.C. is also acknowledged with thanks. The constructive comments by the referee are also acknowledged with thanks.

References

Axford, W. I., & Reid, G. C. 1963, JGR, 68, 1793
Bai, T. 1992, ApJ, 388, L69
Burlaga, L. F., & Ogilvie, K. W. 1969, JGR, 74, 2815
Choudhary, D. P., Lawrence, J. K., Norris, M., & Cadavid, A. C. 2014, SoPh, 289, 649
Chowdhury, P., Choudhary, D. P., Gosain, S., & Moon, J. 2015, Ap&SS, 356, 7
Chowdhury, P., Khan, M., & Ray, P. C. 2014, SoPh, 289, 649
Forbush, S. E. 1937, PhRv, 51, 1108
Gerand, V. B. 1959, JGR, 64, 593
Gonzalez, L. C., & Gonzalez, W. D. 1987, JGR, 92, 4357
Jian, L.K., Russell, C. T., & Luhmann, J. G. 2011, SoPh, 274, 321
Kaynano, M. T., & Kousky, V. E. 2002, Tell, 51A, 373
Kilcik, A., Rozelot, J.-P., & Ozguc, A. 2024, Univ, 10, 107
Kudela, K., & Sabbah, I. 2016, Sci, 59, 547
Lara, A., Andrea Borgazzi, O., Jr, Mendes, R. R., & Domingues, M. O. 2008, SoPh, 248, 155
Lou, Y.-Q., Wang, Y.-M., Fan, Z., Wang, S., & Wang, J.X. 2003, MNRAS, 345, 809

Madden, R. A., & Julian, P. R. 1971, JAtS, 28, 702
Meyer, P., & Simpson, J. A. 1955, PhRv, 99, 1517
Modzelewska, R., & Alania, M. V. 2013, SoPh, 286, 513
Morlet, J., Arens, G., Forgeau, I., & Giard, D. 1982, Geop, 47, 203
Mursula, K., & Zieger, B. 2000, AdSpR, 25, 1939
Mursula, K., Zieger, B., & Vilppola, J. H. 2003, SoPh, 212, 201
Nayar, S. R. P., Nair, V. S., Radhika, V. N., & Revathy, K. 2001, SoPh, 201, 405
Nayar, S. R. P., Radhika, V. N., Revathy, K., & Ramadas, V. 2002, SoPh, 208, 359
Oliveira, D. M., & Raeder, J. 2015, JGR, 120, 4313
Pirjola, R. 1982, Geoph, 18, 1
Rieger, E., Kanbach, G., Reppin, C., et al. 1984, Natur, 312, 623
Shen, C., Chi, Y., Wang, Y., Xu, M., & Wang, S. 2017, JGR, 122, 5931
Simpson, J. A., Fonger, W., & Treiman, S. B. 1953, PhRv, 90, 934
Singh, Y. P. 2020, E&SS, 7, e2019EA001068
Singh, Y. P., & Badruddin 2006, SoPh, 234, 339
Singh, Y. P., & Badruddin 2024, Ap&SS, 369, 66
Singh, Y. P., Badruddin, B., & Agarwal, S. 2024, AdSpR, 74, 5252
Singh, Y. P., Badruddin, & Gautam, S. 2012, JASTP, 89, 48
Takeuchi, T., Russell, C. T., & Araki, T. 2002, JGR, 107, A12
Torrence, C., & Compo, G. C. 1998, BAMS, 79, 61
Tsurutani, B. T., & Hajra, R. 2021, JSWSC, 11, 23
Verma, V. K., & Joshi, G. C. 1994, SoPh, 155, 401
Venkatesan, D., & Badruddin 1990, SSRv, 52, 121
Wilken, B., Goertz, C. K., Baker, D. N., Higbie, P. R., & Fritz, T. A. 1982, JGR, 87, 5901
Wilson, C. R., & Sugiura, M. 1961, JGR, 66, 4097
Wu, C. C., & Lepping, R. P. 2008, AdSpR, 41, 335
Zhang, J., Richardson, I. G., Webb, D. F., et al. 2007, JGR, 112, A10